Molecular Biology of the Cell
Vol. 16, 2091–2105, April 2005

Cholesterol and Fatty Acids Regulate Dynamic Caveolin Trafficking through the Golgi Complex and between the Cell Surface and Lipid Bodies[V]

Albert Pol,*† Sally Martin,* Manuel A. Fernández,† Mercedes Ingelmo-Torres,† Charles Ferguson,* Carlos Enrich,† and Robert G. Parton*

*Institute for Molecular Bioscience, Centre for Microscopy and Microanalysis and School of Biomedical Sciences, University of Queensland, Queensland 4072, Australia; and †Departament de Biologia Cellular, Facultat de Medicina, Institut d'Investigacions Biomèdiques August Pi Sunyer, Universitat de Barcelona, 08036 Barcelona, Spain

Submitted August 25, 2004; Revised January 18, 2005; Accepted January 21, 2005
Monitoring Editor: Benjamin Glick

Caveolins are a crucial component of plasma membrane (PM) caveolae but have also been localized to intracellular compartments, including the Golgi complex and lipid bodies. Mutant caveolins associated with human disease show aberrant trafficking to the PM and Golgi accumulation. We now show that the Golgi pool of mainly newly synthesized protein is detergent-soluble and predominantly in a monomeric state, in contrast to the surface pool. Caveolin at the PM is not recognized by specific caveolin antibodies unless PM cholesterol is depleted. Exit from the Golgi complex of wild-type caveolin-1 or -3, but not vesicular stomatitis virus-G protein, is modulated by changing cellular cholesterol levels. In contrast, a muscular dystrophy-associated mutant of caveolin-3, Cav3P104L, showed increased accumulation in the Golgi complex upon cholesterol treatment. In addition, we demonstrate that in response to fatty acid treatment caveolin can follow a previously undescribed pathway from the PM to lipid bodies and can move from lipid bodies to the PM in response to removal of fatty acids. The results suggest that cholesterol is a rate-limiting component for caveolin trafficking. Changes in caveolin flux through the exocytic pathway can therefore be an indicator of cellular cholesterol and fatty acid levels.

INTRODUCTION

Caveolins have been well studied as structural components of plasma membrane (PM) caveolae. Moreover, caveolins have been described in the Golgi complex (Kurzchalia and Parton, 1999; Gkantiragas *et al*., 2001); the endoplasmic reticulum (ER)/Golgi network (Smart *et al*., 1994); *cis*-Golgi cisternae (Luetterforst *et al*., 1999); *trans*-Golgi network (TGN)-derived vesicles of epithelial cells (Kurzchalia *et al*., 1992; Scheiffele *et al*., 1998); cytosolic lipid bodies (Fujimoto *et al*., 2001; Ostermeyer *et al*., 2001; Pol *et al*., 2001); endosomes (Pol *et al*., 1999; Gagescu *et al*., 2000); and in a novel endocytic compartment, the caveosome (Pelkmans *et al*., 2001; Nichols, 2003). Little is known about whether these proteins can, under physiological conditions, cycle to/from these intracellular compartments. Conformational changes of the caveolin protein, and possibly the interaction with other proteins or lipids, have complicated analysis of the tracking of the protein between different cellular pools (Dupree *et al*., 1993; Luetterforst *et al*., 1999; Nomura and Fujimoto, 1999). Caveolin is a fatty acid- and cholesterol-binding protein. It can be phosphorylated on several residues, apparently interacts with a long and diverse list of proteins, and forms high-molecular-weight homo- and hetero-oligomers (Monier *et al*., 1995; Murata *et al*., 1995; Sargiacomo *et al*., 1995; Trigatti *et al*., 1999). Questions also remain about the importance of a soluble form of caveolin-1 and the role of cytosolic trafficking in caveolin dynamics (Uittenbogaard *et al*., 1998). Real-time studies of caveolins have overcome some of these difficulties but vary in their conclusions regarding caveolin dynamics and trafficking (Mundy *et al*., 2002; Thomsen *et al*., 2002). Generally, the surface pool of caveolin-1 seems to be relatively immobile unless cells are perturbed experimentally (e.g., okadaic acid addition or actin depolymerization) or cells are incubated with viruses that cause caveolae (and caveolin-1) internalization (Parton *et al*., 1994; Pelkmans *et al*., 2001). However, a Golgi pool of caveolin has been well-documented and implicated in epithelial sorting (Kurzchalia *et al*., 1992; Dupree *et al*., 1993). The importance of understanding caveolin trafficking is evident from the finding that aberrant caveolin trafficking underlies human disease conditions. Caveolin-3 mutants associated with human muscle disease conditions such as limb girdle muscular dystrophy type 1C accumulate within the Golgi complex and act in a dominant manner to perturb

This article was published online ahead of print in *MBC in Press* (http://www.molbiolcell.org/cgi/doi/10.1091/mbc.E04–08–0737) on February 2, 2005.

[V] The online version of this article contains supplemental material at *MBC Online* (http://www.molbiolcell.org).

Address correspondence to: Robert G. Parton (r.parton@imb.uq.edu.au) or Albert Pol (apols@ub.edu).

Abbreviations used: BHK, baby hamster kidney; Cav^{DGV}, caveolin 3 DGV truncation; CD, cyclodextrin; Cyhx, cycloheximide; ER, endoplasmic reticulum; FRAP, fluorescence recovery after photobleaching; GFP, green fluorescent protein; HA, hemagglutinin; LB, lipid body; PM, plasma membrane; TGN, *trans*-Golgi network; TX-100, Triton X-100; VSV-G, vesicular stomatitis virus-G protein.

Table 1. Antibodies used in this work and summary of the specificity of the antibodies for the different pools of caveolin under different fixation and permeabilization procedures (see text and Figure 1 for details)

Antibodies			Caveolin pool detected		
Classification	Antibody	Reference	Method	Golgi	PM
Anti-Go-cav	MoTL37120	BD Transduction Laboratories C37120	PFA/saponin	+	−
			PFA/TX-100	−	−
			Methanol	−	+
	Con-cav	Luetterforst *et al*. (1999)	PFA/saponin	+	−
			PFA/TX-100	−	−
			Methanol	−	+
	MoZYMED	Zymed Laboratories 03-6000	PFA/saponin	+	−
			PFA/TX-100	−	−
			Methanol	−	+
	Mocav2	BD Transduction Laboratories C57820	PFA/saponin	+	−
			PFA/TX-100	−	−
			Methanol	−	+
Anti-PM-cav	MoTL43420	BD Transduction Laboratories C43420	PFA/saponin	−	+
			PFA/TX-100	−	+
			Methanol	−	+
Anti-cav	RbTL	BD Transduction Laboratories C13630	PFA/saponin	+	+
			PFA/TX-100	−	+
			Methanol	−	+

trafficking of wild-type caveolin-3 to the PM (Galbiati *et al*., 1999). For example, the P104L mutant of caveolin-3, Cav3P104L, has a short half-life and undergoes ubiquitination and proteasome-dependent degradation (Galbiati *et al*., 2000). An equivalent mutation in caveolin-1, P132L, was reported to occur in 16% of human breast cancers and shown to have similar aberrant trafficking (Hayashi *et al*., 2001; Lee *et al*., 2002). The mechanisms underlying trafficking of caveolin through the Golgi complex, the role of vesicular versus cytosolic traffic, and the nature of the block in trafficking of mutant caveolin proteins are presently unknown. Moreover, recent studies showing that wild-type (WT)-caveolin can associate with lipid bodies (LBs) in a reversible and lipid-regulated manner (Pol *et al*., 2004) suggests that caveolin can be directed into other trafficking pathways.

In the present study, we have characterized a number of antibodies that specifically label the intracellular pool of the protein. We show that newly synthesized caveolins transit the Golgi complex before being transported to the PM. Exit from the Golgi complex and association with the PM are accompanied by oligomerization, acquisition of detergent insolubility, and masking of specific caveolin epitopes; caveolin at the PM is not recognized by specific caveolin antibodies unless cholesterol is depleted. Moreover, we now show that caveolin transport from the Golgi complex can be regulated by lipids; transport of WT-caveolins, but not the Cav3P104L mutant or a control transmembrane protein, is accelerated by cholesterol addition. We also have characterized the trafficking of caveolin to lipid bodies by using fluorescent caveolin constructs and fluorescence recovery after photobleaching (FRAP). Caveolin redistributes from the PM to LBs in response to fatty acids, illuminating a novel pathway of communication between these two compartments. In addition, caveolin within LBs can associate with the PM, suggesting that caveolin can move bidirectionally between these two membrane systems in response to specific environmental stimuli.

MATERIALS AND METHODS

Plasmids, Antibodies, and Reagents

Cav3-green fluorescent protein (GFP) and Cav3P104L-GFP were generated as described previously (Luetterforst *et al*., 1999). Vesicular stomatitis virus-G protein (VSV-G)-GFP was kindly provided by Dr. J. Lippincott-Schwartz (National Institutes of Health, Bethesda, MD). Primary caveolin antibodies used in this work are summarized in Table 1. Mouse anti-GM130 was obtained from BD Transduction Laboratories (Lexington, KY). Mouse and rabbit anti-hemagglutinin (HA) were kindly provided by Prof. David James (University of Queensland, Queensland, Australia) and Dr. Tommy Nilsson (European Molecular Biology Laboratory, Heidelberg, Germany). Gold-conjugated secondary antibodies were from Jackson ImmunoResearch Laboratories (West Grove, PA). Alexa Fluor-conjugated secondary antibodies were from Molecular Probes (Eugene, OR). Horseradish peroxidase (HRP)-conjugated secondary antibodies were from Zymed Laboratories (South San Francisco, CA). Cycloheximide (Cyhx), 2-hydroxypropyl-β-cyclodextrin (CD), filipin, and water-soluble cholesterol (Chl) were purchased from Sigma-Aldrich (St. Louis, MO).

Cell Culture and Cyhx/Cholesterol Treatments

Baby hamster kidney cells (BHK) and Vero cells were maintained in DMEM with 10% (vol/vol) fetal calf serum (FCS) supplemented with 2 mM L-glutamine, 50 U/ml penicillin, and 50 μg/ml streptomycin sulfate. Then, 16 h before the experiments, the cells were split in fresh 10% FCS medium supplemented with 2 mM L-glutamine. Cells were transfected using LipofectAMINE Plus (Invitrogen, Paisley, United Kingdom) according to the manufacturer's instructions. In some experiments, 10 μg/ml Cyhx (from a 10 mg/ml stock solution in 100 mM HEPES, pH 7.5) was added directly to the growth medium for different times. For cholesterol addition, cells were incubated with 30 μg/ml cholesterol prepared freshly from a powdered stock (15.1 mg of cholesterol per gram of solid) and premixed at room temperature for 30 min in DMEM by gentle agitation. When Cyhx and cholesterol (or CD) were used in combination, both were dissolved in DMEM. For the experiments performed at 15 or 20°C, Cyhx, CD, and cholesterol were dissolved in CO_2-independent medium (Invitrogen). For those experiments, control incubations at 37°C also were performed in air medium but out of the CO_2 incubator. Cyhx completely inhibited protein synthesis as judged by the lack of any detectable fluorescence after expression of GFP in the presence of Cyhx for 24 h. In some experiments, cells were preincubated in a medium containing 50 μg/ml oleic acid (Calbiochem, San Diego, CA) conjugated with fatty acid-free bovine serum albumin (Calbiochem) and incubated in the same medium for the time of the transfection as described previously (Pol *et al*., 2004).

Immunofluorescence Microscopy: Whole Cells

BHK cells grown on glass coverslips were fixed with either methanol (−20°C for 2 min) or 4% paraformaldehyde (PFA; room temperature for 1 h). PFA-

fixed cells were then washed twice in phosphate-buffered saline (PBS) and permeabilized for 10 min with either 0.1% saponin (wt/vol) or 0.1% Triton X-100 (TX-100) (vol/vol) at room temperature. They were then labeled as described previously (Pol *et al.*, 2004). Filipin staining was performed as described previously (Pol *et al.*, 2001). To quantify the fluorescence intensity, images corresponding to the different treatments performed in parallel were captured at the same contrast and intensity and the pixel intensity analyzed using NIH Image software. A total of 200 cells from random fields were analyzed for each treatment.

Immunofluorescence Microscopy: PM Sheets

For the preparation of PM sheets, 3T3-L1 adipocytes were grown and differentiated on coverslips as described previously (Frost and Lane, 1985). Cells were disrupted by sonication using a Sonifier 250 (Branson Ultratronics, Danbury, CT) in cold sonication buffer (20 mM HEPES, pH 7.2, 120 mM potassium glutamate, 20 mM potassium acetate, and 10 mM EGTA) supplemented with 0.5 mM dithiothreitol and 250 μM phenylmethylsulfonyl fluoride as described previously (Robinson *et al.*, 1992). PM sheets were fixed using either 4% PFA in PBS for 30 min at room temperature or methanol for 2 min at –20°C. For extraction of cholesterol, PM sheets were incubated in sonication buffer in the absence or presence of 0.4% methyl-β-cyclodextrin for 30 min at 37°C before fixation in 4% PFA. Plasma membrane sheets were labeled by indirect immunofluorescence microscopy as described previously.

Immunoprecipitation and Western Blotting

Seventy-five percent confluent, 6.5-cm dishes of BHK cells were washed twice with cold PBS before being extracted for 2 min by immersion into 1 ml of ice-cold 10 mM Tris, pH 7.5, 150 mM NaCl, and 5 mM EDTA, and protease and phosphatase inhibitors, supplemented with 0.1% TX-100. Nuclei and unbroken cells were removed of the soluble supernatant by centrifugation at 2000 rpm for 5 min at 4°C in an Eppendorf Microfuge. The amount of extracted protein was quantified by the method of Bradford (1976). Two micrograms of antibody was mixed with 120 μg of sample in a final volume of 500 μl for 2 h at 4°C. Antibody/caveolin complexes were harvested using 40 μl of protein A/G bound to Sepharose beads for an additional 45 min. Finally, the complexes were pelleted and washed twice before eluting using 40 μl of SDS-PAGE electrophoresis buffer. For Western blotting analysis, equal volumes of each immunoprecipitation were electrophoretically separated by SDS-PAGE in 12% polyacrylamide gels. Polypeptides were transferred to Immobilon membranes (Millipore, Billerica, MA), and proteins were detected using specific antibodies diluted in PBS containing 2% nonfat dry milk. After washing in PBS solution containing 0.1% Tween 20, primary antibodies were detected by using HRP-conjugated secondary antibodies diluted in 2.5% nonfat dry milk in PBS. Finally, the reaction was developed by using the enhanced chemiluminescence system (Amersham Biosciences UK, Little Chalfont, Buckinghamshire, United Kingdom).

Oligomerization Gradients

Seventy-five percent confluent 6.5-cm dishes of BHK cells were washed twice with cold PBS before being extracted for 2 min by immersion into 1 ml of ice-cold 10 mM Tris, pH 7.5, 150 mM NaCl, and 5 mM EDTA, and protease and phosphatase inhibitors, supplemented with 0.1% TX-100. Nuclei and unbroken cells were removed of the soluble supernatant by centrifugation at 2000 rpm for 5 min at 4°C in an Eppendorf Microfuge. Samples were loaded at the top of discontinuous sucrose gradient ranging from 5 to 45% sucrose (freshly prepared in Tris-based buffer). The gradients were centrifuged for 18 h at 40,000 rpm in a SW-50.1 rotor (Beckman Coulter, Fullerton, CA), and finally 10 fractions were unloaded from the top. Each fraction of the gradient was further immunoprecipitated with an anti-Golgi-caveolin (anti-Go-cav) or with anti-PM-cav as described previously.

Photobleaching Experiments and Time-Lapse Videomicroscopy

FRAP experiments were carried out using a Leica TCS SL laser scanning confocal spectral microscope (Leica Microsystems Heidelberg, Mannheim, Germany) with argon and HeNe lasers attached to a Leica DMIRE2 inverted microscope equipped with an incubation system with temperature and CO_2 control. For visualization of GFP, images were acquired using 63× oil immersion objective lens (numerical aperture 1.32), 488-nm laser line, excitation beam splitter RSP 500, emission range detection 500–600 nm, and the confocal pinhole set at 2–3 Airy units to minimize changes in fluorescence efficiency due to proteins/structures-GFP moving away from the plane of focus. The whole Golgi/lipid bodies/cytoplasm area of a protein transfected cell was photobleached using 50–80 scans with the 488-nm laser line at full power in a region of interest. Pre- and postbleach images were monitored at different intervals for different times. The excitation intensity was attenuated down to ~5% of the half laser power to avoid significant photobleaching. Fluorescence recoveries in the bleached region and overall photobleaching in the whole cell during the series were quantified using the Image Processing Leica confocal software. Background fluorescence was measured in a random field outside of the cells. Fluorescence values were normalized following the methods described previously (Phair and Misteli, 2000; Dundr *et al.*, 2002). This expression accounts for the small loss in total intensity caused by the bleach itself and yields a more accurate estimate of the immobile fraction.

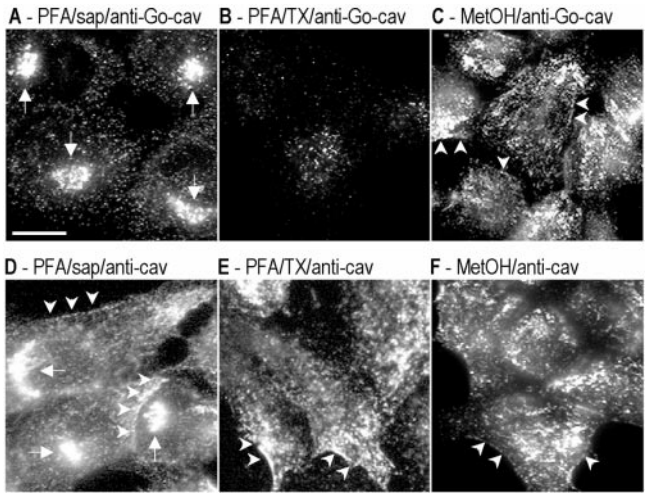

Figure 1. Specific antibodies show affinity for different pools of caveolin. BHK cells were processed for immunofluorescence microscopy by using different fixation (PFA/methanol) and permeabilization (saponin/TX-100) protocols. Caveolin distribution was analyzed with two different polyclonal antibodies: anti-Go-cav antibody (A–C) and anti-cav antibody (D–F). Golgi-associated caveolin was detected with both antibodies in cells fixed with PFA and permeabilized with saponin (A and D) but not in cells fixed in methanol (C and F) or permeabilized with Triton X-100 (B and E). PM-associated caveolin was detected for anti-caveolin antibody in all three experimental conditions (D–F). The anti-Go-caveolin antibody only detected the PM-associated caveolin when the cells were fixed with methanol (C) but not PFA (A and B). In total, six antibodies were tested. See Table 1 for a summary of the results and details of antibodies and protocols. Bar, 5 μm.

RESULTS

Epitopes of PM-associated Caveolin Are Unmasked upon Cholesterol Extraction or Methanol Solubilization

We have previously shown that certain caveolin antibodies exclusively recognize the Golgi pool of the protein and not the PM pool. This specificity is maintained even upon overexpression of caveolin to high levels (Luetterforst *et al.*, 1999). In this work, we investigated this specificity further, to gain insights into the changes associated with the transport of caveolin to the PM.

A total of six anti-caveolin antibodies were tested in BHK cells. By Western blotting all the antibodies showed similar recognition of caveolin (our unpublished data). In contrast, by immunofluorescence the antibodies showed specificity for different pools of caveolin. PFA/saponin was used as our standard fixation and permeabilization method. Representative staining is shown in Figure 1 (see summary in Table 1). Under these conditions, all antibodies could be classified as recognizing exclusively the Golgi pool of caveolin (here termed anti-Go-cav), the PM pool (anti-PM-cav), or both Golgi and PM pools (anti-cav). For example, the con-cav antibody (anti-Go-cav) only recognized caveolin associated with the Golgi complex (Figure 1A, arrows), whereas the rbTL antibody (anti-cav) recognized caveolin present on both the Golgi complex and the PM (Figure 1D, arrowheads). The specificity of the antibodies for the caveolin-1 protein was tested in Fischer rat thyroid (FRT) cells, which lack caveolin-1 (Zurzolo *et al.*, 1994). In FRT

cells, the antibodies used in this study (with the exception of the anti-caveolin-2 reactive antibodies) showed negligible labeling (our unpublished data).

To investigate the reason for the different staining patterns, different fixation/permeabilization conditions were used with the above-mentioned antibodies. Cells fixed with PFA and permeabilized with TX-100 showed a dramatically reduced Golgi staining with all the antibodies (Figure 1B), but the anti-cav or anti-PM-cav antibodies still detected PM caveolin (Figure 1E, arrowheads). This suggests that the Golgi pool of caveolin is sensitive to the fixation/permeabilization conditions because antibodies against the Golgi marker GM130 showed a similar efficiency of labeling in all three fixation/permabilization conditions (our unpublished data). The most striking findings were obtained with methanol as the fixation/permeabilization method. Under these conditions, all antibodies (including anti-Go-cav antibodies) showed PM staining (Figure 1, C and F).

In view of the documented cholesterol binding properties of caveolin (Murata *et al*., 1995) and the above-mentioned finding that PM caveolin epitopes were revealed upon methanol fixation, we investigated whether extraction of cholesterol from the PM would allow normally Golgi-specific antibodies to label the PM pool. 3T3-L1 adipocytes have abundant caveolae, and sheets of PMs can be easily prepared from these cells (Robinson *et al*., 1992). Cells grown on glass coverslips were sonicated and the remaining PM attached to the coverslip fixed using either PFA or methanol before labeling with either anti-cav or anti-Go-cav antibodies. As in intact cells, only anti-cav antibodies detected caveolin on the PFA-fixed PM sheets, showing that the specificity observed in intact cells was maintained (Figure 2B). In contrast, when the PM sheets were fixed with methanol (Figure 2A), or treated with CD (to extract cholesterol) for 10 min before fixation with PFA, PM-associated caveolin was now recognized by the anti-Go-cav antibody (Figure 2D) as efficiently as with the anti-cav antibody (Figure 2, B and D). As a control, labeling with specific antibodies against syntaxin 4 was shown to be unaffected by the different treatments (Figure 2, A and D). Note that anti-caveolin antibodies detect caveolae over the entire PM lawn (which are not resolved and thus exhibit diffuse labeling) as well as caveolae associated with large plasma membrane invaginations of the PM. The latter look like rings and contain other PM markers such as syntaxin 4 (Parton *et al*., 2002). From these experiments, we conclude that caveolin delivery to the PM renders caveolin unreactive to specific antibodies, but this can be reversed by cholesterol depletion.

We tested whether acute depletion of cholesterol in living cells causes a similar effect. BHK cells were treated for 2 h with 2% CD, and the extraction of cholesterol was visualized by means of filipin staining. Even after 2 h, surface cholesterol was still visible (Figure 2, E and F). This treatment did not expose surface epitopes detected with the anti-Go antibody (Figure 2, G and H). These data suggest that cells have mechanisms to move cholesterol to the PM and therefore maintain higher levels of cholesterol than we achieve by treating isolated PM sheets with CD. Interestingly, we noted that cells treated with CD showed stronger caveolin labeling of the Golgi complex (Figure 2H). When the relative fluorescence was quantified, CD-treated cells showed an increase of 65% in Golgi caveolin-associated fluorescence (from 1.9 $\pm$ 0.7 to 3.1 $\pm$ 1.1; Figure 2I; also see Figure 5), but the Golgi marker GM130 was unaffected (our unpublished data). This result raised the possibility that cholesterol regulates the exit of caveolin from the Golgi complex.

Transit of Newly Synthesized Caveolin through the Golgi Complex

We took advantage of the specificity of the anti-Go-cav antibodies for the Golgi-associated caveolin to more closely examine the traffic of the protein through this compartment. BHK cells were incubated for different times with a general inhibitor of protein translation, Cyhx, and the Golgi-associated pool of caveolin were monitored by means of an anti-Go-cav antibody. A reduction in the amount of protein (59 $\pm$ 16%) was evident after 1 h of incubation with Cyhx (Figure 3, B and G, for quantification), and caveolin was almost undetectable (10 $\pm$ 8%) after 3 h (Figure 3C). Interestingly, even after prolonged incubation with Cyhx, a low level of caveolin was detected in the Golgi complex of some cells. This may represent a permanent or recycling pool of the protein as Cyhx caused a complete block in protein synthesis as shown in control experiments (our unpublished data). When cells were incubated with Cyhx at 15°C (which inhibits both ER/Golgi transport and post-Golgi transport) or 20°C (which inhibits post-Golgi transport), no detectable reduction in the levels of caveolin in the Golgi was observed (our unpublished data). This is consistent with exit of a significant fraction of caveolin from the Golgi complex via a membrane trafficking pathway, but further work is required to examine whether a vesicular transport pathway is involved. These results also demonstrate that accessibility of caveolin to the antibodies is not modified during the incubation with Cyhx. Further support for this comes from the observation that the anti-cav antibody no longer detects the protein in the Golgi complex after Cyhx treatment (our unpublished data). Very similar kinetics was obtained in response to puromycin, a different inhibitor of protein translation (our unpublished data).

Next, we analyzed the movement of the newly synthesized caveolin to the Golgi complex. BHK cells were incubated for 3 h with Cyhx, to clear the biosynthetic pool of caveolin, then the drug washed out allowing caveolin expression to resume. After recovery at 37°C, caveolin reappeared in the Golgi complex (Figure 3D). The recovery (quantified as percentage of pixel intensity with respect to control cells; Figure 3G) reached half of the original intensity after 30 min (43 $\pm$ 12) (Figure 3D). This recovery was completely blocked at 15°C (Figure 3F) but not at 20°C (Figure 3E).

Caveolin in the Golgi Complex Is in Low-Molecular-Weight Oligomers and Is Soluble in Triton X-100 at Low Temperature

To confirm and extend the results obtained by immunofluorescence microscopy, we developed a biochemical method to isolate Golgi caveolin. We took advantage of the fact that the Golgi-associated pool of caveolin in unfixed cells is soluble in a low concentration of TX-100 at low temperature, in contrast to the PM-associated protein that is largely, but not completely, insoluble (see below). For these experiments, BHK cells were extracted at 4°C with a buffer containing 0.1% TX-100. Under these conditions the Golgi-associated caveolin was largely extracted (compare Figure 4A with B, and E with F) compared with caveolin on the PM as judged by immunofluorescence microscopy (compare Figure 4C with D, and E with F). Therefore, cells were treated for 1, 2, or 3 h with Cyhx at 37 or 20°C and extracted in 0.1% TX-100. After extraction, the soluble protein was immunoprecipitated with an anti-Go-cav antibody (see *Materials and Methods* for details). In agreement with the results shown in Figure 3, the amount of caveolin solubilized from the Golgi decreased progressively in response to Cyhx (Figure 4G).

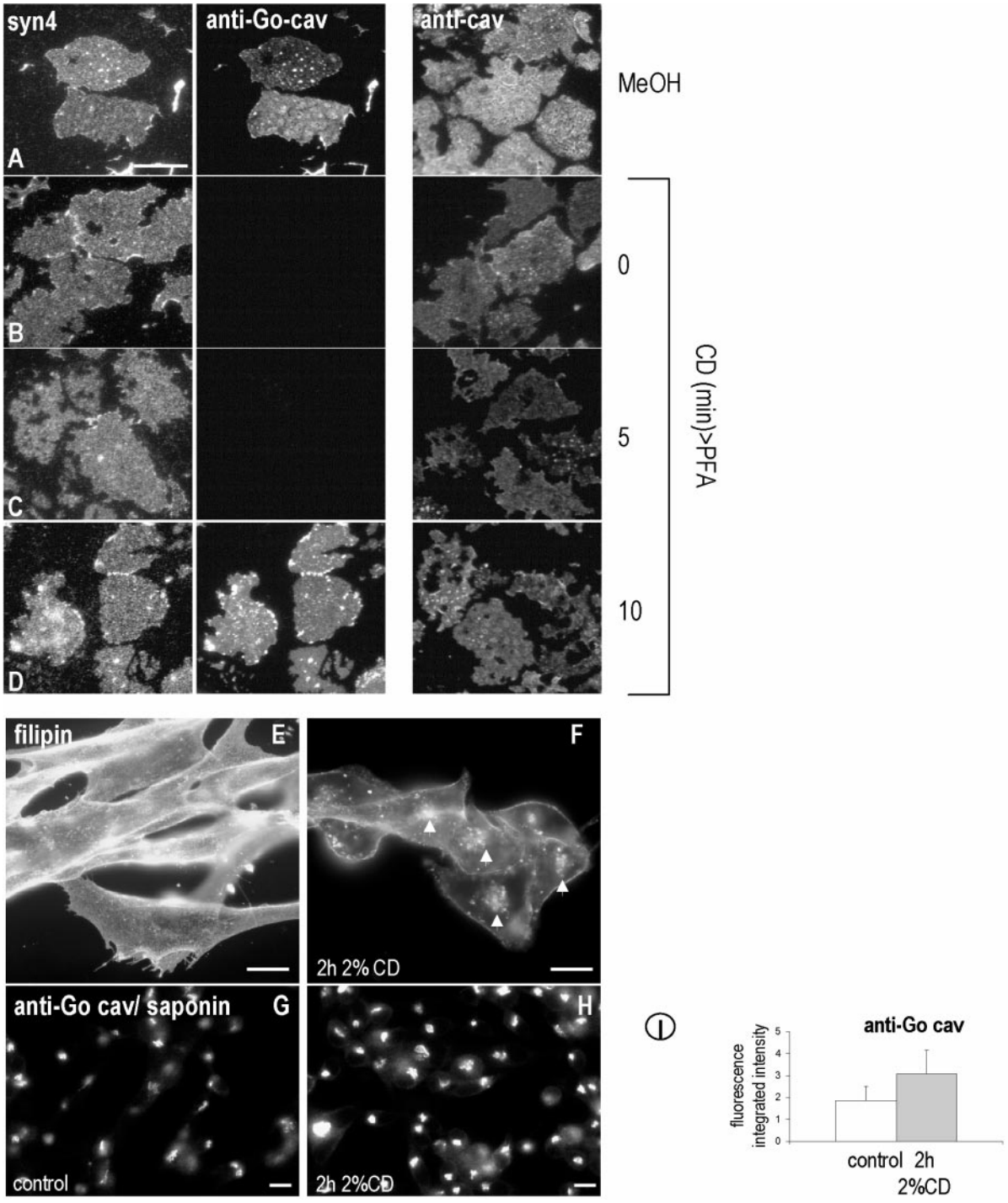

Figure 2. Cholesterol depletion reveals specific epitopes of caveolin. Plasma membrane sheets were prepared from 3T3-L1 adipocytes and fixed immediately in MeOH (A) or PFA (B) or incubated in 0.4% CD for 5 min (C) or 10 min (D) before PFA fixation. Membranes were single-labeled using anti-cav or double-labeled using anti-Go-cav and anti-syntaxin4. Anti-cav recognized caveolin on the PM in both PFA- and MeOH-fixed membranes. Anti-Go-cav recognized caveolin on the PM only when the membranes were fixed with MeOH (E) or extracted with CD for 10 min before fixation with PFA (D), whereas anti-Syn4 labeled both PFA- and MeOH-fixed membranes. (E–I) BHK were treated for 2 h with 2% CD, and the distribution of cholesterol was studied by means of filipin (F). Even after 2 h, surface cholesterol was still visible (compare E with F). After the CD treatment, and in contrast to the results obtained for plasma membrane sheets, anti-Go-cav do not recognized caveolin on the PM (H); however, a stronger caveolin labeling of the Golgi complex was observed (compare H with G). (I) The relative fluorescence associated with caveolin in the Golgi-complex was quantified in control and CD-treated cells. CD-treated cells showed an increase of 65% in Golgi caveolin-associated fluorescence. Bar, 5 μm.

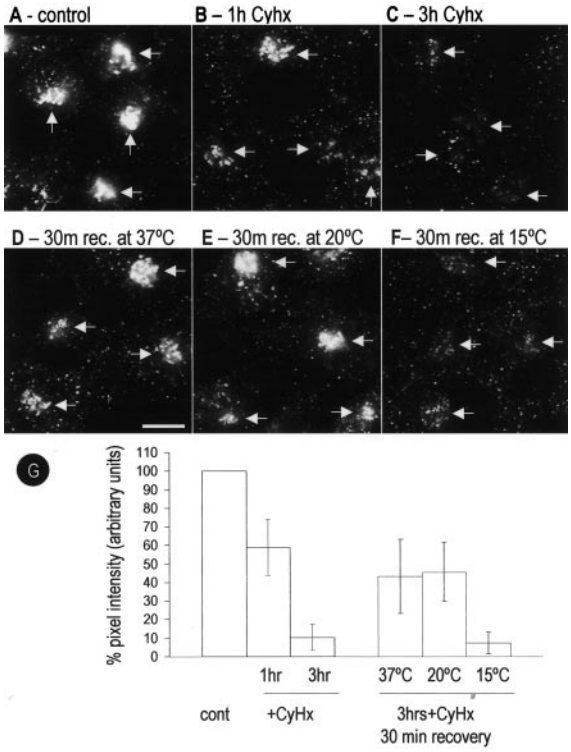

Figure 3. Golgi-associated caveolin predominantly corresponds to newly synthesized protein. BHK cells were incubated for different times with Cyhx (a general inhibitor of protein translation), and the Golgi-associated pool of caveolin was monitored by means of an anti-Go-cav antibody. The amount of caveolin present in the Golgi complex was quantified as percentage of pixel intensity with respect to control cells (G). A reduction to 59± 16 or 10 ± 8% in the amount of caveolin was detected after 1 h (B) or 3 h (C), respectively. Next, the cells were incubated for 3 h with Cyhx, and the drug was washed out, allowing the cells to recover. After 30 min at 37°C, 43 ± 12% of caveolin reappeared in a the Golgi complex (D). The recovery was completely blocked at 15°C (7 ± 1%) (F) but unaffected at 20°C (46 ± 14%) (E). Bar, 5 μm.

When the cells were incubated at 20°C for 3 h, the amount of caveolin immunoprecipitated increased consistent with continued traffic from the ER but reduced exit from the Golgi. No change in immunoprecipitated caveolin was observed in response to incubations with Cyhx in cells maintained at 20°C. In addition, no changes in immunoprecipitated caveolin was observed when the extracted material was immunoprecipitated with an anti-PM-cav antibody after various times of Cyhx treatment (Figure 4H). These results validate the isolation method which was then used to specifically study the properties of Golgi-associated caveolin.

Control cells or cells treated for 3 h with Cyhx were extracted by immersion in a buffer that contained 0.1% TX-100 at 4°C, and the soluble supernatant was fractionated using a sucrose gradient to separate the different molecular weight oligomers of caveolin (see *Materials and Methods* for details). Fractions were unloaded from the top of the gradient, and each fraction was immunoprecipitated using anti-Go-cav or anti-PM-cav. Finally, the caveolin immunoprecipitated from each fraction was detected by Western blotting (Figure 4I). The anti-Go-cav antibody recognized predominantly low-molecular-weight oligomers of the protein (fractions 1 and 2 of the gradient). In agreement with the results shown previously, the caveolin pool recognized by the anti-Go-cav antibody diminished in response to the treatment with Cyhx. In contrast, the anti-PM-cav antibody exclusively recognized the high-molecular-weight caveolin complexes (fractions 3–5). Although PM-associated caveolin is largely insoluble in the detergent, a small amount of high-molecular-weight oligomers of caveolin that was not affected by the presence of Cyhx was present in the soluble supernatant. This pool of protein, presumably released by mechanical extraction rather than being soluble in the detergent, was used as a control for the specificity of the anti-Go antibodies.

Cholesterol Modulates Caveolin Traffic through the Golgi Complex

Caveolin is both a cholesterol and fatty acid binding protein and has been suggested to be involved in the intracellular transport of lipids. In view of the above-described studies suggesting that Golgi exit is associated with cholesterol binding, we investigated whether cholesterol modulates caveolin traffic by taking advantage of the above-mentioned methods to look at the Golgi-associated caveolin pool.

Cells were incubated for 2 h in a medium enriched in cholesterol. Protein translation was inhibited using Cyhx, and the transport of caveolin out of the Golgi complex was monitored using the anti-Go-cav antibody. In the presence of elevated cholesterol, the rate of decrease in the Golgi caveolin pool observed after treatment with Cyhx was accelerated from 25 ± 9 to 11 ± 3% (Figure 5, D and E, for quantification). We calculated that the half-life of Golgi caveolin was 70 min in control cells in contrast to 42 min in cells treated with cholesterol (Figure 5E). The findings were confirmed using a biochemical approach. Cells were incubated with cholesterol for 90 min, and the amount of soluble caveolin that could be immunoprecipitated by the anti-Go-cav antibody was determined as described in Figure 4. In agreement with the immunofluorescence microscopy less caveolin was present in the Golgi complex of cells treated with cholesterol, accelerating the effect of Cyhx (Figure 5F). The changes promoted by cholesterol addition were inhibited at 20°C, suggesting that cholesterol modulates the exit of caveolin out of the Golgi complex. In contrast, and in accordance with the data shown in Figure 2, when the cells were treated with 2% CD (to deplete cholesterol), more caveolin accumulated in the Golgi complex, reducing the effect of Cyhx (Figure 5G).

Time-Lapse Videomicroscopy of Caveolin Traffic through the Golgi Complex

To extend these results and to examine whether a noncaveolar membrane protein shows similar changes in transport, we directly studied the transport of a GFP-tagged caveolin-3 construct compared with the transport of the raft-excluded VSV-G tagged with GFP by time-lapse videomicroscopy. Caveolin-GFP constructs traffic to caveolae in an identical manner to wild-type caveolins (Pelkmans *et al*., 2001, 2002; Thomsen *et al*., 2002). Caveolin-3 also associates with caveolae when expressed in nonmuscle cells (Way and Parton, 1995), but it has the advantage of not oligomerizing with endogenous caveolin-1 (Song *et al*., 1997). The proteins were transfected into BHK cells, and after 6 h cells were selected for the presence of Cav3-GFP or VSV-G-GFP in the Golgi area. At this very short time point after the transfection, caveolin and VSV-G were commonly observed in the Golgi complex. Next, Cyhx or a combination of Cyhx/cholesterol was added to the media, and images were captured at intervals of 20 min. After 60-min incubation with Cyhx, the levels of Golgi-associated caveolin decreased to 59 ± 1% of the initial levels (see representative experiment in Figure 6, A and B). Identical results were obtained when a C-terminally yellow fluorescent protein-tagged caveolin 1 was studied (our unpublished data). In agreement with

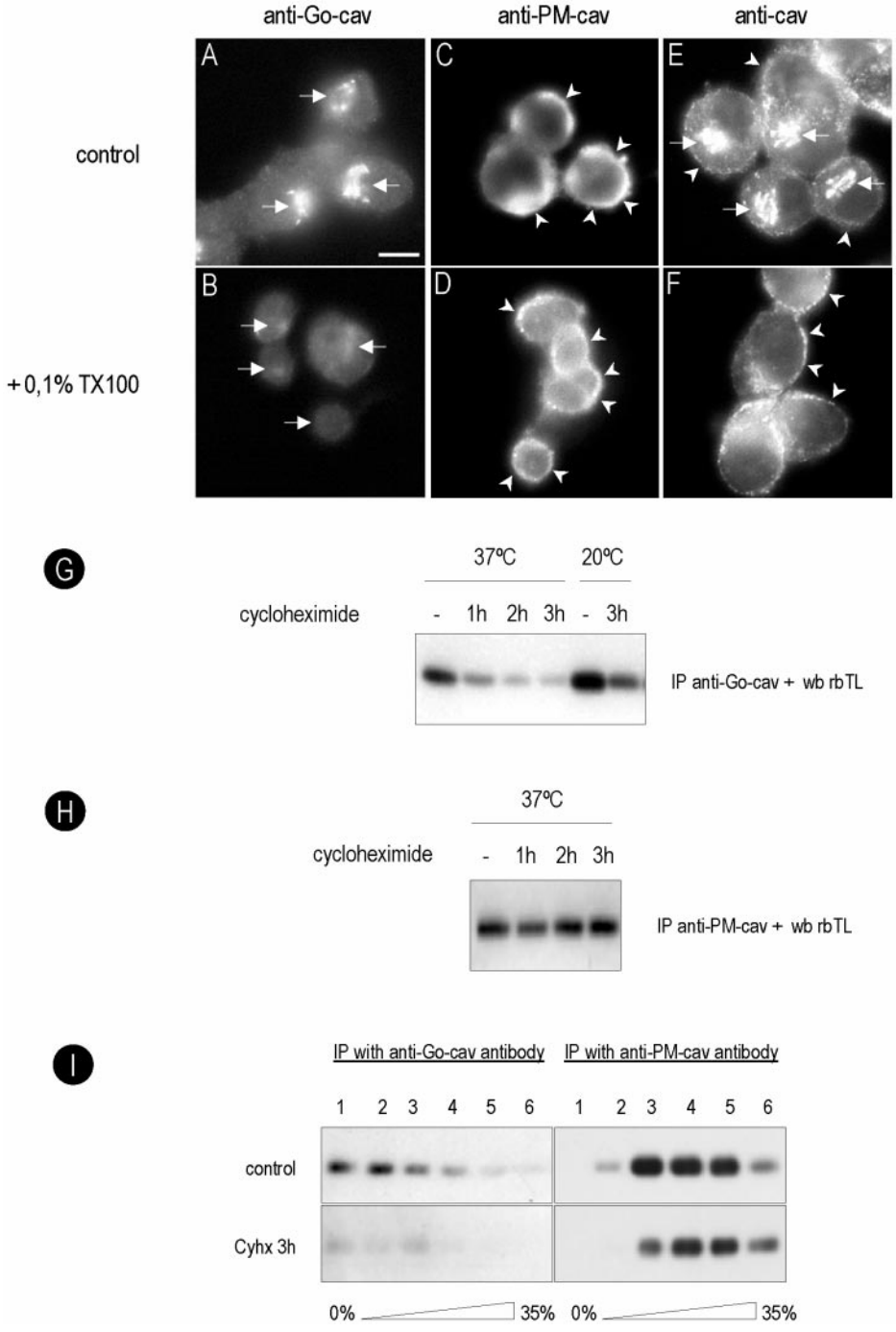

Figure 4. Golgi caveolin is detergent soluble and forms low-molecular-weight oligomers. BHK cells were extracted for 2 min at 4°C with a buffer containing 0.1% TX-100, fixed in PFA, and caveolin was detected with an anti-Go-cav or an anti-PM-cav antibody. The Golgi pool of caveolin was completely extracted by the detergent (compare A and B or E and F), but the PM pool was largely unaffected (compare C and D or E and F). In G, BHK cells were treated for 1, 2, or 3 h with Cyhx at 37 or 20°C, extracted for 2 min at 4°C with a buffer containing 0.1% TX-100, and the soluble fraction was immunoprecipitated with anti-Go-cav antibody. The amount of caveolin decreased progressively in response to Cyhx, and little protein was detected after 3 h. When the cells were incubated at 20°C, the amount of caveolin immunoprecipitated increased. At 20°C, no effect was observed in response to Cyhx consistent with retention in the Golgi complex. No changes in response to Cyhx were observed with an anti-PM-cav antibody (H). (I) Control cells or cells treated for 3 h with Cyhx were extracted with 0.1% TX-100, and the different molecular weight oligomers of caveolin were fractionated using a sucrose gradient (see *Materials and Methods* for details). Fractions of the gradient were immunoprecipitated using anti-Go-cav or anti-PM-cav. The anti-Go-cav antibody recognized predominantly low-molecular-weight oligomers of the protein (fractions 1 and 2 of the gradient), but the anti-PM-cav antibody exclusively recognized the high-molecular-weight caveolin complexes (fractions 3–5). In contrast to the PM pool of the protein, Golgi caveolin was sensitive to Cyhx. Bar, 5 μm.

the results shown in Figures 4 and 5, treatment with Cyhx and cholesterol further diminished the levels of caveolin in the Golgi complex to 27 ± 6% (Figure 6, C and D; also see average quantitation and time course in Figure 6E). In the presence of Cyhx, the levels of Golgi-associated VSGV were reduced to 74 ± 12% of the initial levels, indicating that VSV-G transits more slowly than caveolin through the Golgi complex. In striking contrast to caveolin, cholesterol addition did not accelerate the transport of VSV-G (71 ± 14%; see quantification in Figure 6E).

Next, we compared the trafficking of wild-type Cav3 to the trafficking of an epitope-tagged form of Cav3P104L, a caveolin mutant associated with muscle diseases that shows aberrant trafficking through the Golgi complex (see Introduction). Cav3P104L accumulated in the Golgi complex when expressed in BHK cells (our unpublished data) as observed in other nonmuscle cells (Galbiati *et al.*, 1999). We used time-lapse videomicroscopy to examine whether the transport of the mutant caveolin out of the Golgi complex is affected by cholesterol addition. As shown in Figure 6, F and G, when the cells were treated with Cyhx, Cav3P104L-GFP was less stable than the wild-type protein and diminished after 1 h to 31 ± 5% of the original intensity. In striking contrast to the wild-type protein (Figure 6, H and I), cholesterol addition retarded the loss of the mutant protein from the Golgi complex (54 ± 6%) (see Figure 6J for the quantitation of 6 experiments), consistent with an

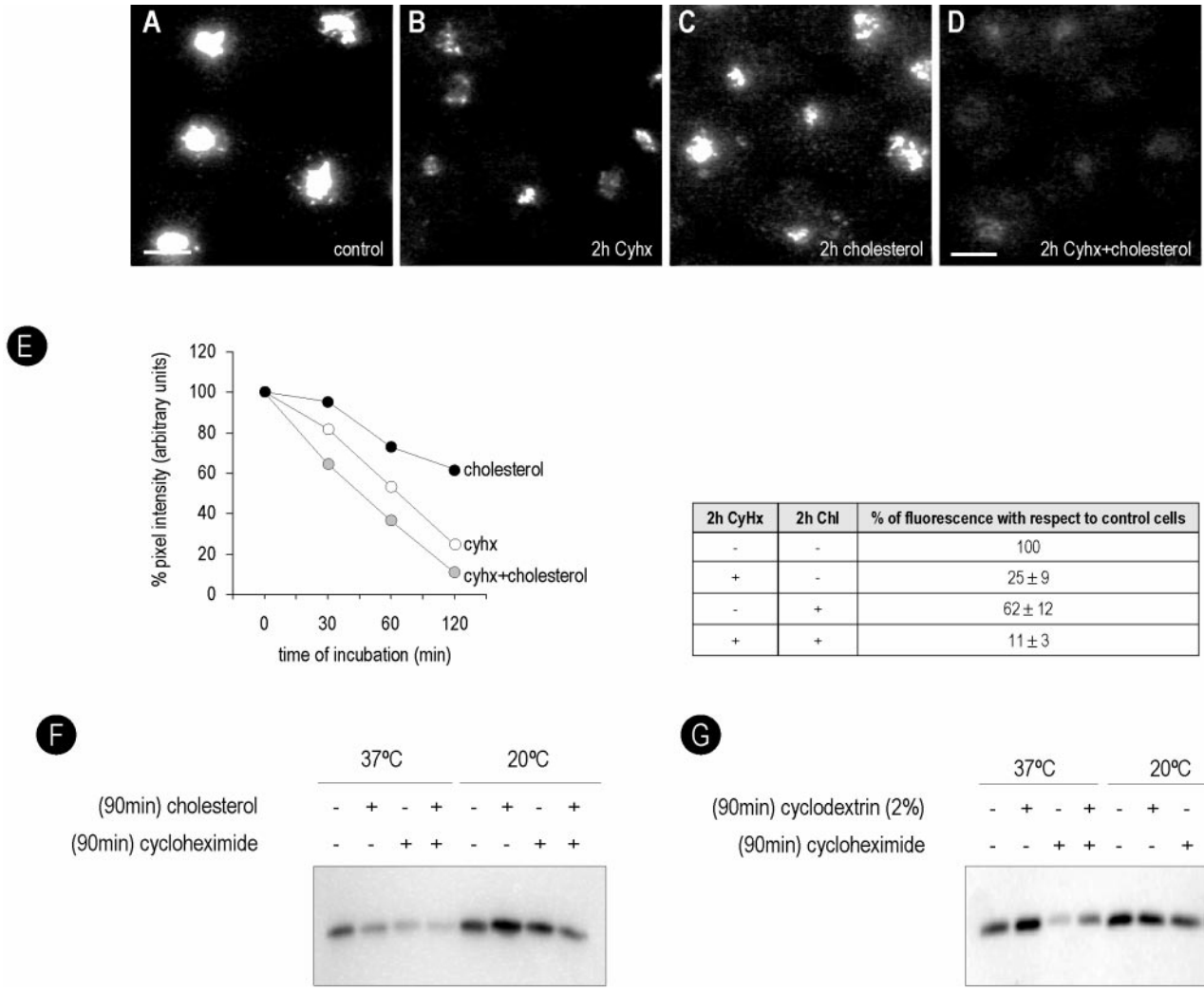

Figure 5. Cholesterol modulates caveolin traffic through the Golgi complex. BHK cells were incubated for 2 h in a medium enriched in cholesterol (C), with CyHx (B) or with both (D). The Golgi-associated caveolin was monitored by means of anti-Go-cav antibody. In the presence of elevated cholesterol, the rate of decrease in the Golgi caveolin pool observed after treatment with Cyhx was accelerated from 25 ± 9 to 11 ± 3% (D and E for quantification). (F and G) Cells were incubated for 90 min with cholesterol or cyclodextrin, Cyhx, or both, and detergent-soluble caveolin was immunoprecipitated by anti-Go-cav antibody. Less caveolin was precipitated from cells treated with cholesterol. However, few changes in the amount of caveolin were observed when the Golgi exit was blocked at 20°C. (G) In contrast, more caveolin was immunoprecipitated from cells treated with 2% CD. Bar, 5 μm.

effect of cholesterol on Golgi exit and/or on stability of the Cav3P104L protein.

FRAP of Golgi-associated Caveolin

The above-mentioned results demonstrate that the Golgi-associated pool of caveolin is mainly derived from newly synthesized protein that transits the Golgi complex in a process regulated by cholesterol. Next, we investigated the post-Golgi trafficking of caveolin by studying the recovery after photobleaching of GFP-tagged caveolin. Cav3-GFP was transfected into Vero cells. After 16 h, the fluorescence of selected cells was photobleached, excluding the Golgi area, and then incubated with Cyhx and cholesterol as described previously (see Video 1 and Figure 7, A and B). Within the first minutes after photobleaching, numerous labeled elements were observed budding from the Golgi complex and trafficking toward the PM (Figure 7D, arrows). Fluorescence at the PM recovered after 10–15 min, and the labeling progressively increased during the rest of experiment (Figure 7, C and D, arrowheads). In agreement with the results obtained by conventional time-lapse videomicroscopy (Figure 6), the Golgi pool of caveolin decreased to 20 ± 5% of the original levels after 1-h incubation in the presence of cholesterol and Cyhx (Figure 7, C and D).

Caveolin Cycles between the PM, the Golgi Complex, and Intracellular Lipid Bodies

So far, we have described the intracellular transport of newly synthesized caveolin through three compartments; from the ER into the Golgi complex and from the Golgi complex, after cholesterol binding and oligomerization of the protein, to the PM. Next, we investigated whether the PM pool of caveolin traffics into other intracellular organelles. It is generally assumed that the pool of caveolin-1 at the cell surface is relatively immobile unless the cells are perturbed experimentally. For example, we have previously

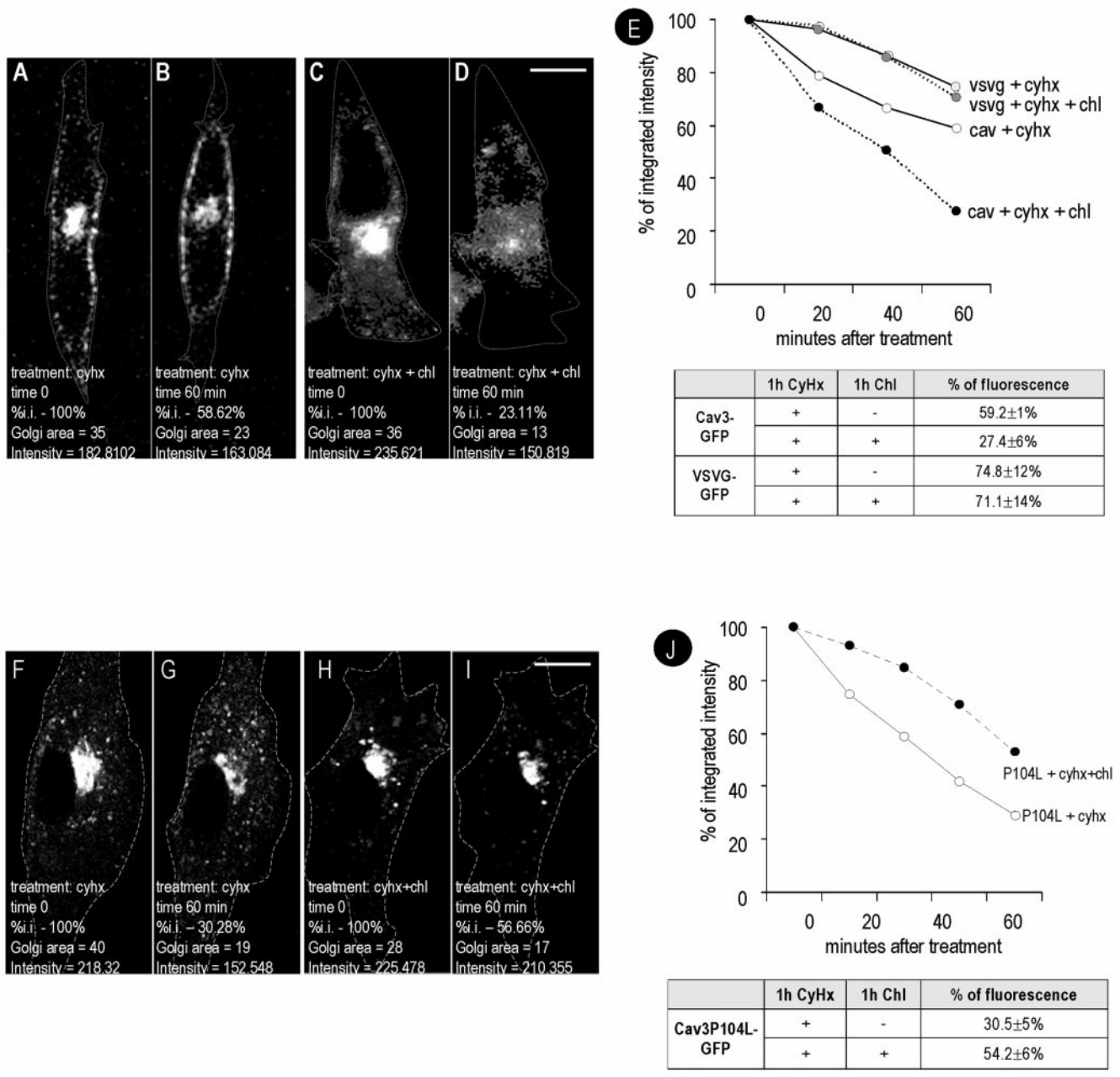

	1h CyHx	1h Chl	% of fluorescence
Cav3-GFP	+	-	59.2±1%
	+	+	27.4±6%
VSVG-GFP	+	-	74.8±12%
	+	+	71.1±14%

	1h CyHx	1h Chl	% of fluorescence
Cav3P104L-GFP	+	-	30.5±5%
	+	+	54.2±6%

Figure 6. Cholesterol increases transport through the Golgi complex of caveolin but not of VSV-G. BHK cells were transfected with Cav3-GFP for 6 h or with VSV-G-GFP induced at 31°C for 3 h. Cells were selected for the presence of the protein in the Golgi area. Next, Cyhx/cholesterol was added to the media. The focus of the microscope was then kept constant during the rest of the experiment. Images were captured every 1 min during 60 min and processed equally to calculate the integrated intensity (the product of the area and the average pixel intensity) (see representative experiment in A–D and average of 6 independent experiments in E). After 1 h, Cav1 levels were reduced to 59 ± 10% in response to Cyhx (compare B with A) and to 27 ± 6% in response to Cyhx/cholesterol (compare D with C and see E for the complete time course). In contrast, no significant differences were observed in the levels of Golgi associated VSV-G after 1 h with Cyhx (75 ± 12%) or with Cyhx/cholesterol (71 ± 14%) (E). (F–J) Cells were transfected with Cav3P104L-GFP and treated with Cyhx or with a combination of Cyhx and cholesterol as described previously (see representative experiment in F–I and average of 6 independent experiments in J). In contrast to the wild-type protein, cholesterol addition retarded the loss of the mutant Cav3P104L-GFP from the Golgi complex (from 30.5 ± 5 to 54.2 ± 6%). Bar, 5 μm.

shown that caveolin accumulates in intracellular LBs in response to the lipid loading of the cells (Pol *et al.*, 2001, 2004).

Cav3-GFP was transfected into BHK cells for 3 h (see scheme of the sequence of treatments in Figure 8). At this time point, the transfected protein was visible in the characteristic tubules of the ER (Figure 8A, open arrows) and in the Golgi complex (Figure 8A, arrowheads). In addition, in some cells, a low level of fluorescence was detected on the PM (Figure 8A, open triangles). Next, the transfection mixture was washed out and replaced by a medium that contained Cyhx to inhibit the

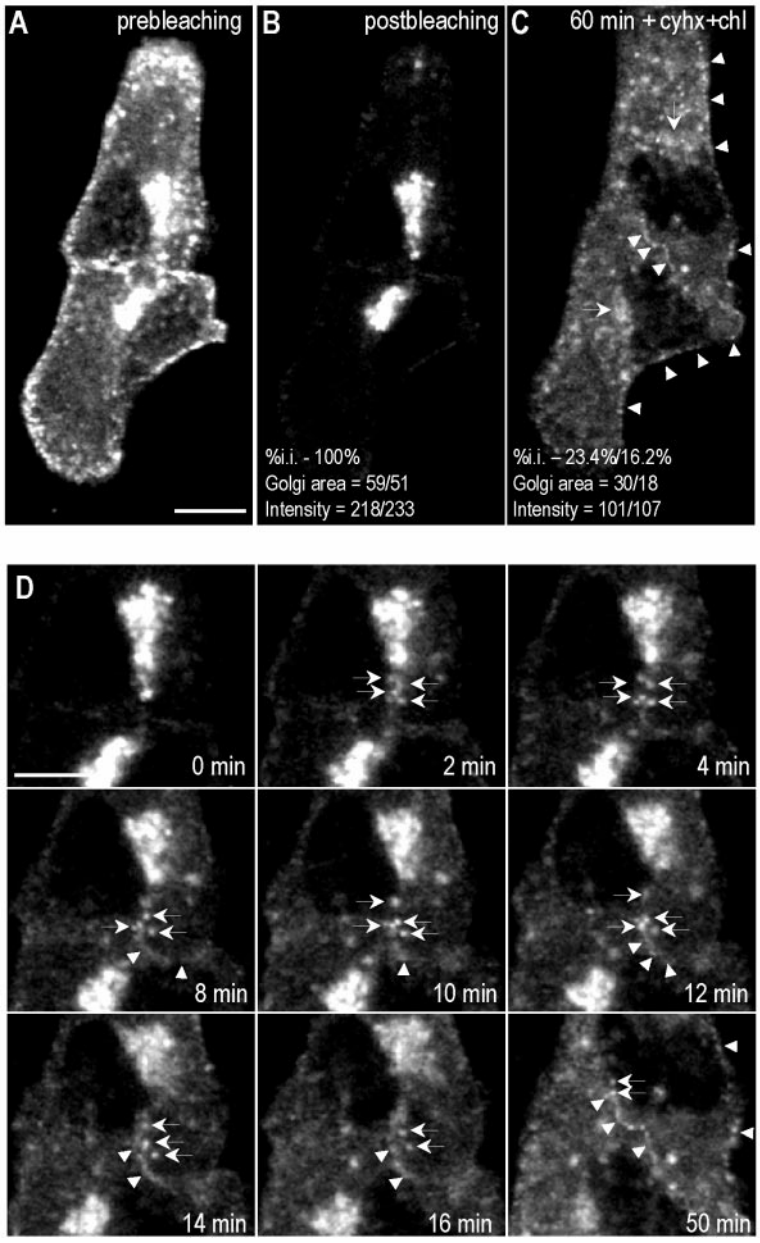

Figure 7. FRAP of Golgi-associated caveolin. Cav3-GFP was transfected into Vero cells. After 16 h, the fluorescence of selected cells (A) was photobleached excluding the Golgi area (B), and then incubated with Cyhx and cholesterol for 1 h (see Video 1). Frames were taken every 10s. Within the first minutes after the photobleaching, numerous vesicles were observed budding from the Golgi complex and trafficking toward the PM (D). Fluorescence at the PM recovered during the experiment (C and D, arrowheads), but Golgi pool of caveolin decreased to 20 ± 5% (C and D). Bar, 5 μm.

synthesis of new protein, and the transfected protein was chased out for 3 h. In agreement with the dynamics of the endogenous protein, caveolin was not visible in the ER or in the Golgi complex but distributed in a characteristic scattered pattern on the PM after 3 h of Cyhx treatment (94 ± 4% of the cells; Figure 8B, open triangles). In a few cells, the transfected protein was permanently retained in the membranes of ER and in intracellular lipid bodies (2 ± 1%) or was still visible in a perinuclear location of the cell (4 ± 1%). At this time point, the cells were incubated with 50 μg/ml oleic acid, in the presence of Cyhx, for an additional 6 h. After the treatment, caveolin was still present on the PM of the cells (96 ± 3% of the cells) (Figure 8B, open triangles), but in addition it was commonly observed on the periphery of intracellular LBs (65 ± 7% of the cells) (Figure 8C, arrows). These results strongly suggest the existence of an intracellular pathway, followed by caveolin, between the PM and LBs.

Next, we analyzed whether caveolin can follow a reverse pathway between the LBs and the PM. For this experiment, Cav3-GFP was transfected for 2 h in the presence of brefeldin A (BFA) to inhibit the exit of the synthesized protein out of the ER. The transfection mixture was washed out and replaced for an additional 2 h by a medium that contained Cyhx and BFA. After this treatment, Cav3-GFP was exclusively detected in lipid bodies (95 ± 1% of the cells; Figure 8D, arrows). Finally, BFA was washed out, and the transfected protein was chased out in the presence of Cyhx. After 2 h, caveolin was still observed in intracellular LBs in few cells (18 ± 5%). However, in the majority of cells (89 ± 14%), the bulk of the protein was present on the PM (Figure 8E, open triangles). In addition to the PM, in 73 ± 8% of the cells, caveolin was observed in the Golgi complex (Figure 8E, arrowheads). Some cells (11 ± 2%) were not able to recover, and caveolin remained exclusively in LBs.

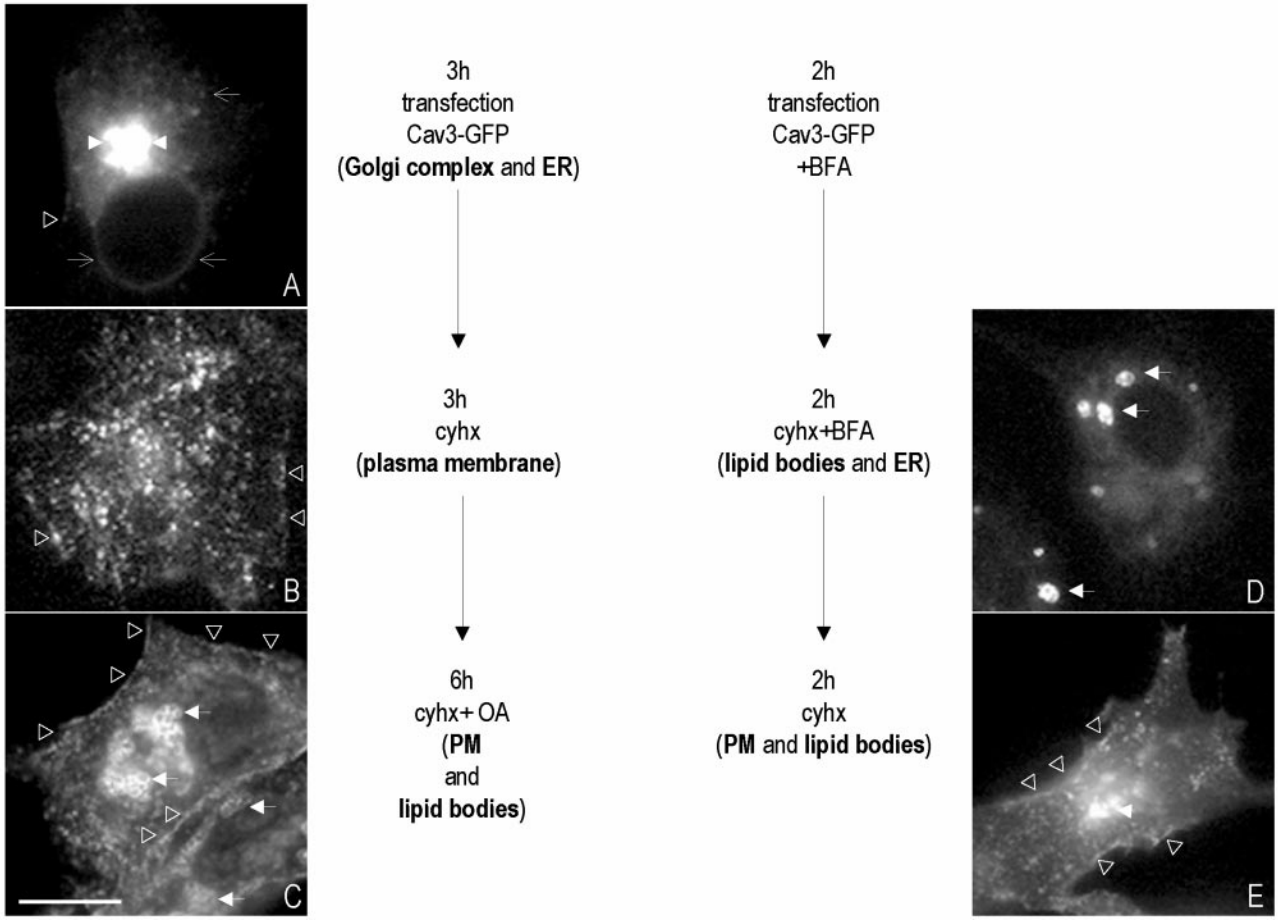

Figure 8. (A–C) Caveolin cycle. (A) BHK cells were transfected with Cav3-GFP for 3 h. (B) Next, the transfection medium was replaced by a medium containing Cyhx, and the cells were incubated for an additional 3 h. (C) Finally, 50 μg/ml oleic acid was added for 6 h. (D and E) BHK cells were transfected with Cav3-GFP for 2 h in the presence of 5 μg/ml BFA. Next, the transfection medium was replaced by medium that contained Cyhx and BFA for an additional 2 h (D). Finally, BFA was washed out, and the cells were further incubated in a media containing Cyhx for 2 h (E). Bar, 5 μm.

Lipid Body-associated Caveolin Represents a Dynamic Pool of the Protein

The above-mentioned results strongly suggest that the same caveolin molecule can cycle between LBs, the PM, and the Golgi complex. This suggests that specific mechanisms must exist for targeting of caveolin to LBs and for retrieval of caveolin in response to changes in the cellular lipid balance. We therefore investigated the dynamics of LB-associated caveolin by using time-lapse videomicroscopy and FRAP.

Vero cells were transfected with Cav3-GFP for 16 h (Figure 9A). At this time point, caveolin was commonly detected in LBs. Caveolin-containing LBs usually aggregated, forming grape-like structures (Figure 9, C and D, and Video 2). To better resolve the dynamics of caveolin in LBs images were captured every 10 s for a total period of 60 min. Two different populations of LBs were observed. One population of LBs only showed a short-range rotary movement (Figure 9E, arrows, and Video 4). The second population showed, in addition, a long range movement underneath the PM (Figure 9E, arrowheads, and Video 4). After photobleaching LB fluorescence recovered rapidly and often reached half of the original intensity in <1 h (Figure 9, F and G, and Video 2). In addition to the translation movement other processes were commonly observed. First, we noted the budding of tubules from LBs that apparently contacted the PM (Figure 9H and Video 3). Second, we observed shuttling of small/group of LBs from larger LBs (Figure 9I and Video 3) and possible fusion processes between LBs (Figure 9J and Video 2).

Finally, we studied the rate of FRAP of LB-associated caveolin (Videos 5 and 6 and Figure 10). In these experiments cells were transfected with cav3-GFP and incubated for 24 h with 50 μg/ml oleic acid to induce the formation of enlarged LBs. Then, cells were completely photobleached, excluding the peripheral PM. Photobleached LBs recovered 21 $\pm$ 3% of the original fluorescence within 1 h (Figure 10, A and B, and Video 5), even in the presence of Cyhx, to inhibit the synthesis of new protein (17 $\pm$ 1%; Figure 10, C and D, and Video 6). To completely clear the biosynthetic pool of caveolin in these experiments, cells were preincubated with Cyhx for 1 h and during the whole experiment. These results clearly demonstrate that the transit of full-length caveolin to and from LBs is extremely dynamic.

DISCUSSION

In this study, we have shown for the first time that the kinetics of transport of caveolin out of the Golgi complex is regulated by cholesterol, suggesting an additional level of complexity in caveo-

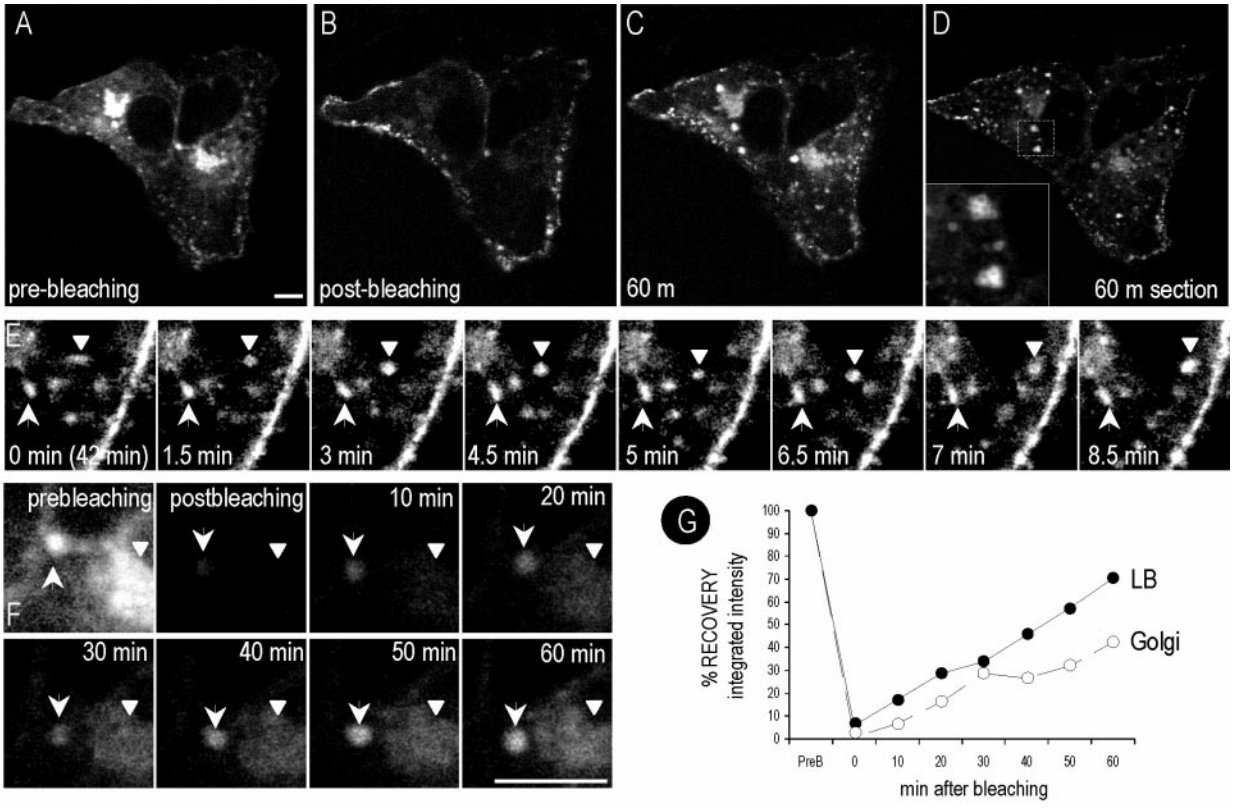

Figure 9.

lin regulation. Delivery of caveolin to the cell surface is associated with loss of reactivity to specific caveolin antibodies, and we now show that this can be reversed by cholesterol depletion. A muscular dystrophy-associated mutant of caveolin-3 is retained in the Golgi complex and in contrast to the wild-type protein is stabilized by cholesterol addition. Moreover, we have shown that caveolin can move from the PM to associate with LBs in response to lipid addition. The LB pool of caveolin is very dynamic and can move to the PM when the lipid source is removed. Thus, caveolin can act as a sensor of cellular lipid levels. This study provides new insights the handling of lipids and the trafficking of caveolin by cells, and it reinforces the importance of lipid bodies as a dynamic cellular organelle.

Cholesterol Depletion Increases PM Reactivity to Specific Caveolin Antibodies

It has been known for some time that specific antibodies to caveolin preferentially label the Golgi pool of the protein. We now show that this is a property of antibodies against several different regions of the protein (N terminus, caveolin scaffolding domain, and C terminus), and the specificity is dependent on the fixation/permeabilization conditions used. We also show for the first time that CD treatment of plasma membrane sheets reveals epitopes in surface caveolin and allows their recognition by these antibodies. This effect was not seen in intact cells, presumably because cellular mechanisms exist to maintain PM cholesterol at higher levels than in CD-treated sheets. A number of effects of cholesterol extraction could explain these results. For example, cholesterol removal could directly expose sites involved in cholesterol binding, cause conformational changes in caveolin, decrease caveolin oligomerization, or remove other raft-associated molecules that interact with caveolin. Oligomerization can occur in the ER, at least in vitro (Monier *et al*., 1995), but the acquisition of detergent insolubility associated with lipid raft localization is thought to occur late in the Golgi complex (Scheiffele *et al*., 1998). In fact, the Golgi pool of caveolin in cultured cells is preferentially removed by detergent preextraction before fixation, suggesting that the bulk of Golgi-associated caveolin is detergent soluble. Intriguingly, a very recent study has shown that a common feature of a range of different caveolin mutants that accumulate in the Golgi complex is their detergent solubility (Ren *et al*., 2004). This is consistent with the idea that lipid raft association might be required for efficient forward transport of caveolin in the Golgi complex, which also would be consistent with the accelerated transport of caveolin in response to cholesterol addition.

Cholesterol Regulates Traffic of Newly Synthesized Protein through the Golgi Complex

Caveolin has been assumed to recycle to the Golgi complex from the cell surface, accounting for the intracellular pool of the protein in the presence of continual exit of caveolins in exocytic vesicles. Consistent with previous studies (Nichols, 2002), we showed that this pool was sensitive to cycloheximide, suggesting that it largely corresponds to newly synthesized protein. This allowed us to follow the transport of endogenous caveolin from its site of synthesis to the PM via the Golgi complex. We found that transport was regulated by the lipid content of the cell. Cholesterol addition accelerates transport through the Golgi complex and cholesterol depletion retards transport. The specificity of this effect was shown by the fact that transport of the nonraft integral membrane protein VSV-G was not affected

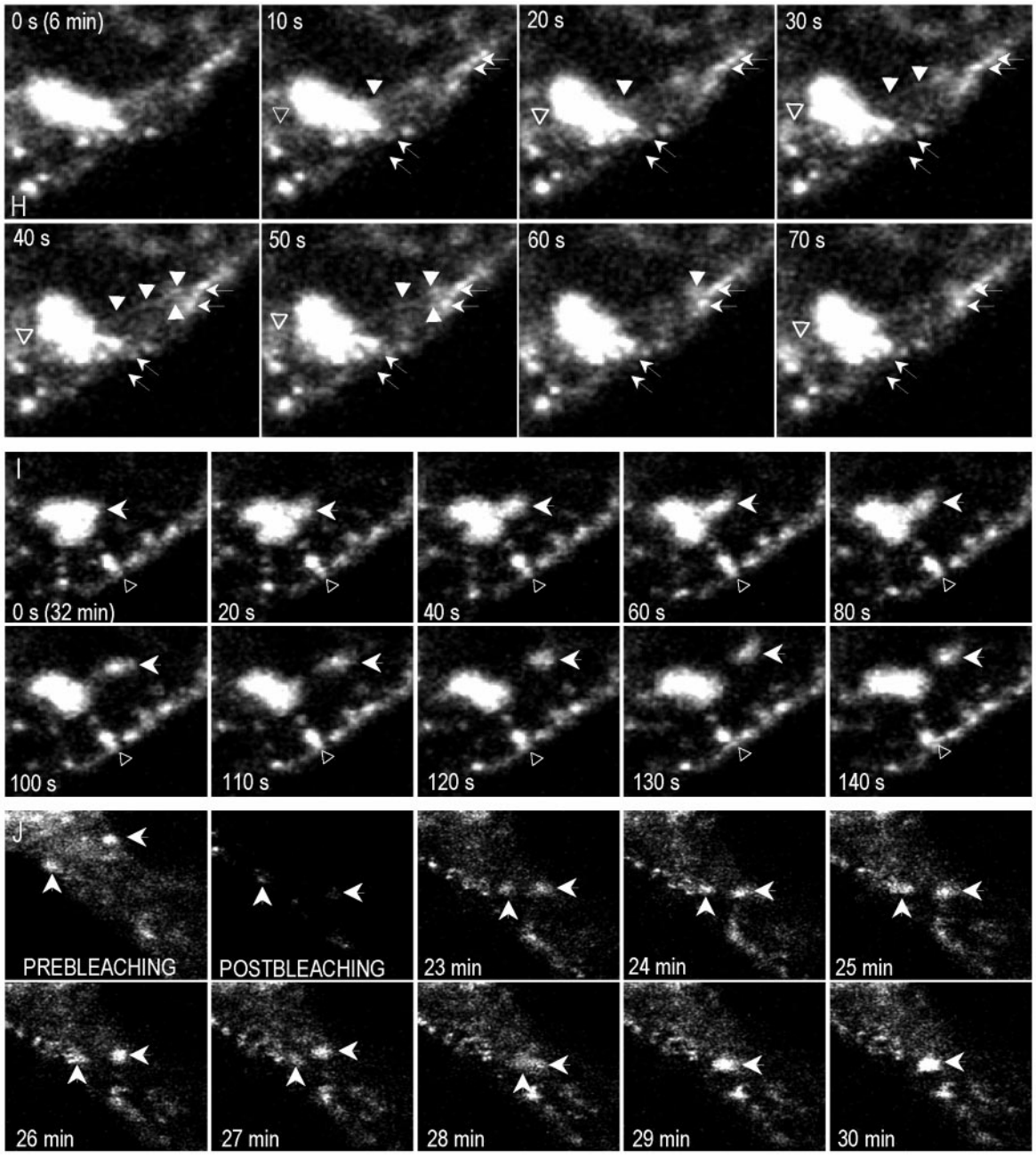

Figure 9 (cont). Time-lapse videomicroscopy and FRAP of LB-associated caveolin. Vero cells were transfected with Cav3-GFP for 16 h (A), after photobleaching of the cell, except the PM (see example in B) images were captured every 10 s for a total period of 60 min. Caveolin containing LBs usually aggregated forming grape-like structures (C, confocal section D, and Video 2). Some LBs showed a short-range rotary movement (E, arrows, and Video 4), whereas others showed a long-range movement underneath the PM (E, arrowheads, and Video 4). After photobleaching, LBs recovered rapidly and often reached half of the original intensity in <1 h (F and G and Video 2). We also noted the budding of tubules from LBs that apparently contacted the PM (H and Video 3), shuttling of small/group of LBs from larger LBs (I and Video 3), and possible fusion processes between LBs (J and Video 2). Bar, 2 μm.

by cholesterol addition. This rules out nonspecific effects of cholesterol on the Golgi complex, as shown in recent studies (Ying *et al*., 2003).

The physiological role of the accelerated transport of caveolin upon cholesterol addition remains to be established, but this is an interesting possibility in view of the reported links between caveolin-1 and cholesterol. We have demonstrated that the expression of a caveolin dominant negative mutant induces a cholesterol imbalance in the cell and reduces the levels of cholesterol on the PM (Pol *et al*., 2001). Caveolin-1 expression is regulated by cholesterol at the transcriptional level (Bist *et al*., 1997, 2000; Fielding *et al*., 1997; Hailstones *et al*., 1998), so cells can respond to changes in free cholesterol. An added level of complexity is shown here; free cholesterol also regulates the amount of caveolin-1 reaching the PM independent of caveolin synthesis. Together with previous studies showing regulation of caveolin-1 protein levels throughout the cell cycle (Fielding *et al*., 1999), this indicates several levels of regulation of caveo-

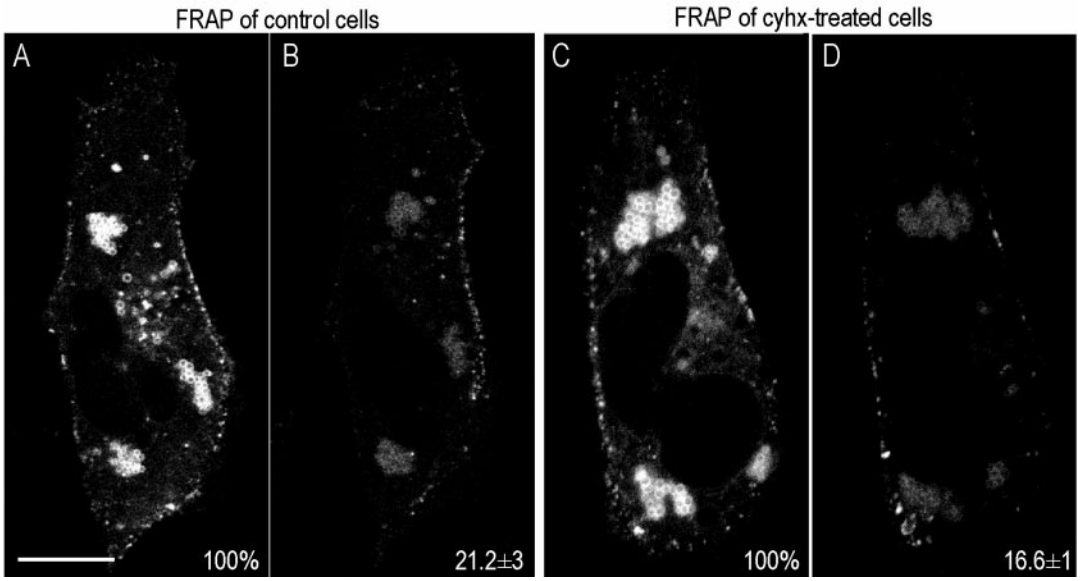

Figure 10. Caveolin cycles between the PM and intracellular lipid bodies. Vero cells were transfected with Cav3-GFP for 24 h in the presence of 50 μg/ml oleic acid. After photobleaching of the cell except the PM, images were captured every 1 min for a total period of 60 min (Videos 5 and 6). Photobleached LBs recovered 21 $\pm$ 3 of the original fluorescence within 1 h (A and B), even in the presence of Cyhx (17 $\pm$ 1, C and D). Bar, 5 μm.

lin by cholesterol. Caveolin-1 could therefore act as a sensitive cholesterol sensor. Increased caveolin expression at the PM may act as a mechanism to increase free cholesterol efflux at early time points of cholesterol increase, which is subsequently followed by increased protein synthesis.

Dynamic and Regulated Two-Way Trafficking of Caveolin between the Cell Surface and Lipid Bodies

Previous studies have shown that caveolin accumulates within LBs in response to fatty acid loading (Liu *et al*., 2004; Pol *et al*., 2004). However, although it is clear that newly synthesized caveolin can reach LBs via the ER (Ostermeyer *et al*., 2001) or via the Golgi complex (Pol *et al*., 2004), is it possible for caveolin to redistribute from the cell surface to LBs? This pathway could play an important role in linking PM lipid levels to the major site of cellular lipid storage, the LB. To test this, we optimized conditions in which caveolin was associated exclusively with the PM pool before fatty acid addition. We observed a striking redistribution of PM caveolin in response to oleic acid. Control experiments showed a complete block in protein synthesis under these conditions arguing against ER-derived caveolin being the source of caveolin in LBs. Using a similar strategy, we examined a related crucial issue; can LB-associated caveolin be retrieved from LBs and reach the PM after fatty acid removal? Our results strongly suggest that this is indeed the case and that the LB is just one potential station in the caveolin cycle. Thus, the LB is not a dead-end, as has been suggested previously, but mechanisms exist to transport caveolin from the LBs.

The elucidation of this caveolin cycle strengthens the proposed role of caveolin and LBs in cellular lipid regulation. However, the mechanisms by which caveolin redistributes in response to fatty acid addition/removal are as yet unclear. The intramembrane region of caveolin has been implicated in LB association (Ren *et al*., 2004). Fatty acids may regulate the exposure of this domain through conformational changes in caveolin or may trigger interactions with other proteins. The results strengthen the view that LBs are a very dynamic structure with traffic to and from these structures. Real-time studies of caveolin trafficking reinforce this view. Cav3-GFP labeled structures constantly bud from the LBs. We also noted proximity of caveolin-containing LBs to the cell surface and apparent interactions with the PM. Our studies raise the possibility that interactions with the PM might facilitate exchange between these two compartments, consistent with the previously proposed view that regulating the lipid composition of the PM may involve caveolins and LBs. The present findings that caveolin can cycle between these two structures, redistributing from one to the other in response to lipid balance, together with previous findings that a caveolin mutant disrupts surface lipid raft domains while associating with, and perturbing LBs (Roy *et al*., 1999; Pol *et al*., 2001, 2004), are all consistent with this hypothesis. Elucidation of the mechanisms involved will prove to be an exciting avenue of future research relevant to both cellular lipid regulation and signal transduction.

ACKNOWLEDGMENTS

We thank Maria Calvo (Serveis Científic-Tècnics, Universitat de Barcelona) for excellent technical assistance in the in vivo confocal microscopy. This work was supported by grants from the National Health and Medical Research Council of Australia and the Human Frontiers Research Progamme to R.G.P. and grants G03/015 from Ministerio de Sanidad y Consumo (Spain), BMC2003-04754 and GEN2003-20662 from Ministerio de Ciencia y Tecnología and Fundació Maratò TV3-2001 to C. E. A. P. is supported by Ramon y Cajal Spanish Research Program (Institut d'Investigacions Biomèdiques August Pi i Sunyer) and Ministerio de Educación y Ciencia (BMC2002-03553 and GEN2003-20662-C07-05/NAC). The Institute for Molecular Bioscience is a Special Research Centre of the Australian Research Council.

REFERENCES

Bist, A., Fielding, C. J., and Fielding, P. E. (2000). p53 regulates caveolin gene transcription, cell cholesterol, and growth by a novel mechanism. Biochemistry *39*, 1966–1972.

Bist, A., Fielding, P. E., and Fielding, C. J. (1997). Two sterol regulatory element-like sequences mediate up-regulation of caveolin gene transcription in response to low density lipoprotein free cholesterol. Proc. Natl. Acad. Sci. USA *94*, 10693–10698.

Bradford, M. M. (1976). A rapid and sensitive method for the quantitation of microgram quantities of protein utilizing the principle of protein-dye binding. Anal. Biochem. *72*, 248–254.

Dundr, M., Hoffmann-Rohrer, U., Hu, Q., Grummt, I., Rothblum, L. I., Phair, R. D., and Misteli, T. (2002). A kinetic framework for a mammalian RNA polymerase in vivo. Science *298*, 1623–1626.

Dupree, P., Parton, R. G., Raposo, G., Kurzchalia, T. V., and Simons, K. (1993). Caveolae and sorting in the trans-Golgi network of epithelial cells. EMBO J. *12*, 1597–1605.

Fielding, C. J., Bist, A., and Fielding, P. E. (1997). Caveolin mRNA levels are up-regulated by free cholesterol and down-regulated by oxysterols in fibroblast monolayers. Proc. Natl. Acad. Sci. USA *94*, 3753–3758.

Fielding, C. J., Bist, A., and Fielding, P. E. (1999). Intracellular cholesterol transport in synchronized human skin fibroblasts. Biochemistry *38*, 2506–2513.

Frost, S. C., and Lane, M. D. (1985). Evidence for the involvement of vicinal sulfhydryl groups in insulin-activated hexose transport by 3T3–L1 adipocytes. J. Biol. Chem. *260*, 2646–2652.

Fujimoto, T., Kogo, H., Ishiguro, K., Tauchi, K., and Nomura, R. (2001). Caveolin-2 is targeted to lipid droplets, a new "membrane domain" in the cell. J. Cell Biol. *152*, 1079–1085.

Gagescu, R., Demaurex, N., Parton, R. G., Hunziker, W., Huber, L. A., and Gruenberg, J. (2000). The recycling endosome of Madin-Darby canine kidney cells is a mildly acidic compartment rich in raft components. Mol. Biol. Cell *11*, 2775–2791.

Galbiati, F., Volonte, D., Minetti, C., Bregman, D. B., and Lisanti, M. P. (2000). Limb-girdle muscular dystrophy (LGMD-1C) mutants of caveolin-3 undergo ubiquitination and proteasomal degradation. Treatment with proteasomal inhibitors blocks the dominant negative effect of LGMD-1C mutants and rescues wild-type caveolin-3. J. Biol. Chem. *275*, 37702–37711.

Galbiati, F., Volonte, D., Minetti, C., Chu, J. B., and Lisanti, M. P. (1999). Phenotypic behavior of caveolin-3 mutations that cause autosomal dominant limb girdle muscular dystrophy (LGMD-1C). Retention of LGMD-1C caveolin-3 mutants within the Golgi complex. J. Biol. Chem. *274*, 25632–25641.

Gkantiragas, I., Brugger, B., Stuven, E., Kaloyanova, D., Li, X. Y., Lohr, K., Lottspeich, F., Wieland, F. T., and Helms, J. B. (2001). Sphingomyelin-enriched microdomains at the Golgi complex. Mol. Biol. Cell *12*, 1819–1833.

Hailstones, D., Sleer, L. S., Parton, R. G., and Stanley, K. K. (1998). Regulation of caveolin and caveolae by cholesterol in MDCK cells. J. Lipid Res. *39*, 369–379.

Hayashi, K., Matsuda, S., Machida, K., Yamamoto, T., Fukuda, Y., Nimura, Y., Hayakawa, T., and Hamaguchi, M. (2001). Invasion activating caveolin-1 mutation in human scirrhous breast cancers. Cancer Res. *61*, 2361–2364.

Kurzchalia, T. V., Dupree, P., Parton, R. G., Kellner, R., Virta, H., Lehnert, M., and Simons, K. (1992). VIP21, a 21-kD membrane protein is an integral component of trans-Golgi-network-derived transport vesicles. J. Cell Biol. *118*, 1003–1014.

Kurzchalia, T. V., and Parton, R. G. (1999). Membrane microdomains and caveolae. Curr. Opin. Cell Biol. *11*, 424–431.

Lee, H., Park, D. S., Razani, B., Russell, R. G., Pestell, R. G., and Lisanti, M. P. (2002). Caveolin-1 mutations (P132L and null) and the pathogenesis of breast cancer: caveolin-1 (P132L) behaves in a dominant-negative manner and caveolin-1 (-/-) null mice show mammary epithelial cell hyperplasia. Am. J. Pathol. *161*, 1357–1369.

Liu, P., Ying, Y., Zhao, Y., Mundy, D. I., Zhu, M., and Anderson, R. G. (2004). Chinese hamster ovary K2 cell lipid droplets appear to be metabolic organelles involved in membrane traffic. J. Biol. Chem. *279*, 3787–3792.

Luetterforst, R., Stang, E., Zorzi, N., Carozzi, A., Way, M., and Parton, R. G. (1999). Molecular characterization of caveolin association with the Golgi complex: identification of a cis-Golgi targeting domain in the caveolin molecule. J. Cell Biol. *145*, 1443–1459.

Monier, S., Parton, R. G., Vogel, F., Behlke, J., Henske, A., and Kurzchalia, T. V. (1995). VIP21-caveolin, a membrane protein constituent of the caveolar coat, oligomerizes in vivo and in vitro. Mol. Biol. Cell *6*, 911–927.

Mundy, D. I., Machleidt, T., Ying, Y. S., Anderson, R. G., and Bloom, G. S. (2002). Dual control of caveolar membrane traffic by microtubules and the actin cytoskeleton. J. Cell Sci. *115*, 4327–4339.

Murata, M., Peranen, J., Schreiner, R., Wieland, F., Kurzchalia, T. V., and Simons, K. (1995). VIP21/caveolin is a cholesterol-binding protein. Proc. Natl. Acad. Sci. USA *92*, 10339–10343.

Nichols, B. (2003). Caveosomes and endocytosis of lipid rafts. J. Cell Sci. *116*, 4707–4714.

Nichols, B. J. (2002). A distinct class of endosome mediates clathrin-independent endocytosis to the Golgi complex. Nat. Cell Biol *4*, 374–378.

Nomura, R., and Fujimoto, T. (1999). Tyrosine-phosphorylated caveolin-1, immunolocalization and molecular characterization. Mol. Biol. Cell *10*, 975–986.

Ostermeyer, A. G., Paci, J. M., Zeng, Y., Lublin, D. M., Munro, S., and Brown, D. A. (2001). Accumulation of caveolin in the endoplasmic reticulum redirects the protein to lipid storage droplets. J. Cell Biol. *152*, 1071–1078.

Parton, R. G., Joggerst, B., and Simons, K. (1994). Regulated internalization of caveolae. J. Cell Biol. *127*, 1199–1215.

Parton, R. G., Molero, J. C., Floetenmeyer, M., Green, K. M., and James, D. E. (2002). Characterization of a distinct plasma membrane macrodomain in differentiated adipocytes. J. Biol. Chem. *277*, 46769–46778.

Pelkmans, L., Kartenbeck, J., and Helenius, A. (2001). Caveolar endocytosis of simian virus 40 reveals a new two-step vesicular-transport pathway to the ER. Nat. Cell Biol. *3*, 473–483.

Pelkmans, L., Puntener, D., and Helenius, A. (2002). Local actin polymerization and dynamin recruitment in SV40-induced internalization of caveolae. Science *296*, 535–539.

Phair, R. D., and Misteli, T. (2000). High mobility of proteins in the mammalian cell nucleus. Nature *404*, 604–609.

Pol, A., Calvo, M., Lu, A., and Enrich, C. (1999). The "early-sorting" endocytic compartment of rat hepatocytes is involved in the intracellular pathway of caveolin-1 (VIP-21). Hepatology *29*, 1848–1857.

Pol, A., Luetterforst, R., Lindsay, M., Heino, S., Ikonen, E., and Parton, R. G. (2001). A caveolin dominant negative mutant associates with lipid bodies and induces intracellular cholesterol imbalance. J. Cell Biol. *152*, 1057–1070.

Pol, A., Martin, S., Fernandez, M. A., Ferguson, C., Carozzi, A., Luetterforst, R., Enrich, C., and Parton, R. G. (2004). Dynamic and regulated association of caveolin with lipid bodies: modulation of lipid body motility and function by a dominant negative mutant. Mol. Biol. Cell *15*, 99–110.

Ren, X., Ostermeyer, A. G., Ramcharan, L. T., Zeng, Y., Lublin, D. M., and Brown, D. A. (2004). Conformational defects slow Golgi exit, block oligomerization, and reduce raft affinity of caveolin-1 mutant proteins. Mol. Biol. Cell *15*, 4556–4567.

Robinson, L. J., Pang, S., Harris, D. S., Heuser, J., and James, D. E. (1992). Translocation of the glucose transporter (GLUT4) to the cell surface in permeabilized 3T3–L1 adipocytes: effects of ATP insulin, and GTP gamma S and localization of GLUT4 to clathrin lattices. J. Cell Biol. *117*, 1181–1196.

Roy, S., Luetterforst, R., Harding, A., Apolloni, A., Etheridge, M., Stang, E., Rolls, B., Hancock, J. F., and Parton, R. G. (1999). Dominant-negative caveolin inhibits H-Ras function by disrupting cholesterol-rich plasma membrane domains. Nat. Cell Biol. *1*, 98–105.

Sargiacomo, M., Scherer, P. E., Tang, Z., Kubler, E., Song, K. S., Sanders, M. C., and Lisanti, M. P. (1995). Oligomeric structure of caveolin: implications for caveolae membrane organization. Proc. Natl. Acad. Sci. USA *92*, 9407–9411.

Scheiffele, P., Verkade, P., Fra, A. M., Virta, H., Simons, K., and Ikonen, E. (1998). Caveolin-1 and -2 in the exocytic pathway of MDCK cells. J. Cell Biol. *140*, 795–806.

Smart, E. J., Ying, Y. S., Conrad, P. A., and Anderson, R. G. (1994). Caveolin moves from caveolae to the Golgi apparatus in response to cholesterol oxidation. J. Cell Biol. *127*, 1185–1197.

Song, K. S., Tang, Z., Li, S., and Lisanti, M. P. (1997). Mutational analysis of the properties of caveolin-1. A novel role for the C-terminal domain in mediating homo-typic caveolin-caveolin interactions. J. Biol. Chem. *272*, 4398–4403.

Thomsen, P., Roepstorff, K., Stahlhut, M., and van Deurs, B. (2002). Caveolae are highly immobile plasma membrane microdomains, which are not involved in constitutive endocytic trafficking. Mol. Biol. Cell *13*, 238–250.

Trigatti, B. L., Anderson, R. G., and Gerber, G. E. (1999). Identification of caveolin-1 as a fatty acid binding protein. Biochem. Biophys. Res. Commun. *255*, 34–39.

Uittenbogaard, A., Ying, Y., and Smart, E. J. (1998). Characterization of a cytosolic heat-shock protein-caveolin chaperone complex. Involvement in cholesterol trafficking. J. Biol. Chem. *273*, 6525–6532.

Way, M., and Parton, R. G. (1995). M-caveolin, a muscle-specific caveolin-related protein. FEBS Lett. *376*, 108–112.

Ying, M., Grimmer, S., Iversen, T. G., Van Deurs, B., and Sandvig, K. (2003). Cholesterol loading induces a block in the exit of VSV-G from the TGN. Traffic *4*, 772–784.

Zurzolo, C., van't Hof, W., van Meer, G., and Rodriguez-Boulan, E. (1994). VIP21/caveolin, glycosphingolipid clusters and the sorting of glycosylphosphatidylinositol-anchored proteins in epithelial cells. EMBO J. *13*, 42–53.